JOURNAL OF MATERIALS SCIENCE **34** (1999) 129–137

The Hertzian contact surface

A. C. FISCHER-CRIPPS
Department of Applied Physics, University of Technology, Sydney, P.O. Box 123, Broadway, NSW 2007, Australia
E-mail: tfc@phys.uts.edu.au.

It is tempting to accept the predictions regarding indentation depth and radius of circle of contact between two elastic bodies in contact given by the well-known Hertz equations at face value. However, it is nevertheless of interest to examine these predictions either by experiment or by independent computation. Indentation depth may be readily compared using standard experimental apparatus but in this paper, attention is given to the radius of curvature of the indented surface for a condition of full load. The conclusion arising from the Hertz equations, that contact between a flat surface and a non-rigid indenter of radius R is equivalent to that between the flat surface and a perfectly rigid indenter of a larger radius, has not thus far been examined in detail in the literature, possibly because of the difficulty in measuring such a radius of curvature *in situ* while load is applied to the indenter. This feature of contact between two solids is of interest since it has been often used as the basis for various hardness theories which involve an elastic–plastic contact. This paper addresses the issue by utilizing the finite-element method to compute the radius of curvature of the contact surface for both elastic and elastic–plastic contacts. It is shown that indentations involving elastic–plastic deformations within either or both the specimen and the indenter are equivalent to indentations with a perfectly rigid spherical indenter whose radius is somewhat smaller than that calculated using the Hertz equations for elastic contact. An experimental compliance response is used to indirectly validate the finite-element results.

1. Introduction

The stresses and deflections arising from the contact between two elastic solids has practical application in hardness testing, wear and impact damage of engineering ceramics, the design of dental prostheses, gear teeth and ball and roller bearings. The contact between a rigid "indenter" and a flat, extensive "specimen" is of particular interest. The shape of the indenter may be spherical, conical, a cylindrical flat punch, or even take the form of a uniformly applied pressure. All such phenomena are usually referred to as "Hertzian contact". The most well-known scenario is the contact between a rigid sphere and a flat surface where Hertz [1, 2] found that the radius of the circle of contact a, is related to the indenter load P, the indenter radius R, and the elastic properties of the materials by

$$a^3 = \frac{4}{3}\frac{kPR}{E} \tag{1a}$$

where k is an elastic mismatch factor given by:

$$k = \frac{9}{16}\left[(1-\nu^2) + \frac{E}{E'}(1-\nu'^2)\right] \tag{1b}$$

In Equation 1b, E, ν and E', ν' are the Young's modulus and Poisson's ratio for the specimen and the indenter, respectively.

Hertz also found that the maximum tensile stress in the specimen occurs at the edge of the contact circle at the surface and is given by

$$\sigma_{\max} = (1-2\nu)\frac{P}{2\pi a^2} \tag{2}$$

This stress, acting in a radial direction on the surface outside the indenter, decreases as the inverse square of the distance away from the center of contact and is usually considered responsible for the production of Hertzian cone cracks. Combining Equations 1 and 2, the maximum tensile stress outside the indenter can be expressed in terms of the indenter radius R

$$\sigma_{\max} = \left(\frac{(1-2\nu)P}{2\pi}\right)\left(\frac{3E}{4k}\right)^{2/3} P^{1/3} R^{-2/3} \tag{3}$$

The mean contact pressure, p_m, is given by the indenter load divided by the contact area, and is a useful normalising parameter which has the additional virtue of having actual physical significance.

$$p_m = \frac{P}{\pi a^2} \tag{4}$$

It can be shown from Equation 1 that the contact area is proportional to $P^{2/3}$ and therefore p_m is proportional

to $P^{1/3}$. Substituting Equation 4 into Equation 1 gives

$$p_m = \left(\frac{3E}{4\pi k}\right)\frac{a}{R} \tag{5}$$

The mean contact pressure may be referred to as the "indentation stress" and the quantity a/R the "indentation strain". Although this definition of "indentation strain" may be questioned, it is appropriate since the elastic strains within the specimen scale with this ratio. For example, without some external reference, it is not possible to tell the difference between indentations made with indenters of different radii if the quantity a/R is the same in each. The functional relationship between p_m and a/R indicates the existence of a stress–strain response similar in nature to that more commonly obtained from conventional uniaxial tension and compression tests. In both cases, a fully elastic condition yields a linear response. However, due to the localized or confined nature of the indentation stress field, an indentation stress–strain relationship yields valuable information about the elastic–plastic properties of the test material which is not generally available from uniaxial tension and compression tests [3].

2. Contact between elastic solids

2.1. Hertz equations

In the following sections, Hertz's original analysis is reviewed for the purposes of gaining an understanding of the process of indentation and the nature of the contact between elastic solids. Particular attention is given to contact involving a spherical indenter. A fully elastic response is assumed first, and later it is shown how the nature of the contact varies when the specimen responds in an elastic–plastic manner.

Following Hertz, the following assumptions serve to facilitate the analysis:

1. The radii of curvature of the contacting bodies are large compared with the radius of the circle of contact. With this assumption, each surface may be treated as an elastic half-space where equations for the stresses and displacements can be found in the literature [4].
2. The dimensions of each body are large compared with the radius of the circle of contact. This allows indentation stresses and strains to be considered independently of those arising from the geometry, method of attachment, and boundaries of each contacting solid.
3. The contacting bodies are in frictionless contact. That is, only a normal pressure is transmitted between the indenter and the specimen. The pressure distribution is given by

$$\frac{\sigma_z}{p_m} = -\frac{3}{2}\left(1 - \frac{r^2}{a^2}\right)^{1/2} \tag{6}$$

Consider now the contact of a sphere of radius R' with elastic modulus E' and Poisson's ratio ν' in contact with the flat surface of a specimen whose elastic constants are E and ν as shown in Fig. 1a. With no load applied, and with the indenter on the point of making contact with the specimen, the distance from a point on the periphery of the indenter and the specimen surface is given by

$$h = \frac{r^2}{2R} \tag{7}$$

where R is the relative curvature of the indenter and the specimen given by

$$\frac{1}{R} = \frac{1}{R'} + \frac{1}{R_S} \tag{8}$$

In Fig. 1a, the load is applied to the indenter in contact with a flat surface (R_S in Equation 8 $= \infty$) such that the point at which load is applied moves a vertical distance δ. This distance is often called the "load-point displacement", and when measured with respect to a distant point in the specimen may be considered the distance of mutual approach between the indenter and the specimen. In general, both the indenter and specimen surface undergo deformation. These deformations are shown by u_z' and u_z at some arbitrary point inside the contact circle for both the indenter and the specimen respectively in the figure. Inspection of Fig. 1a shows that the load-point displacement is given by

$$\delta = u_z' + u_z + h \tag{9}$$

Other combinations of specimen and indenter types are shown in Fig. 1b to d. If the indenter is perfectly rigid, then $u_z' = 0$ (Fig. 1d). For both rigid and non-rigid indenters, $h = 0$ at $r = 0$ and thus the load-point displacement is given by $\delta = u_z' + u_z$. Note that u_z', u_z and h are all functions of r, although the function $u_z(r)$ has yet to be specified precisely.

Hertz showed that a distribution of pressure of the form given by that for a sphere, Equation 6, results in displacements of the specimen surface, for $r \leq a$, as given by [5]

$$u_z = \frac{1-\nu^2}{E}\frac{3}{2}p_m\frac{\pi}{4a}(2a^2 - r^2) \qquad r \leq a \tag{10a}$$

and outside the contact circle $r > a$ [5]

$$u_z = \frac{1-\nu^2}{E}\frac{3}{2}p_m\frac{1}{2a}\left[(2a^2 - r^2)\sin^{-1}\frac{a}{r} + r^2\frac{a}{r}\left(1 - \frac{a^2}{r^2}\right)^{1/2}\right] \tag{10b}$$

After deformation, the contact surface lies in between the two original surfaces and is also part of a sphere whose radius depends on the relative radii of curvature of the two opposing surfaces and elastic properties of

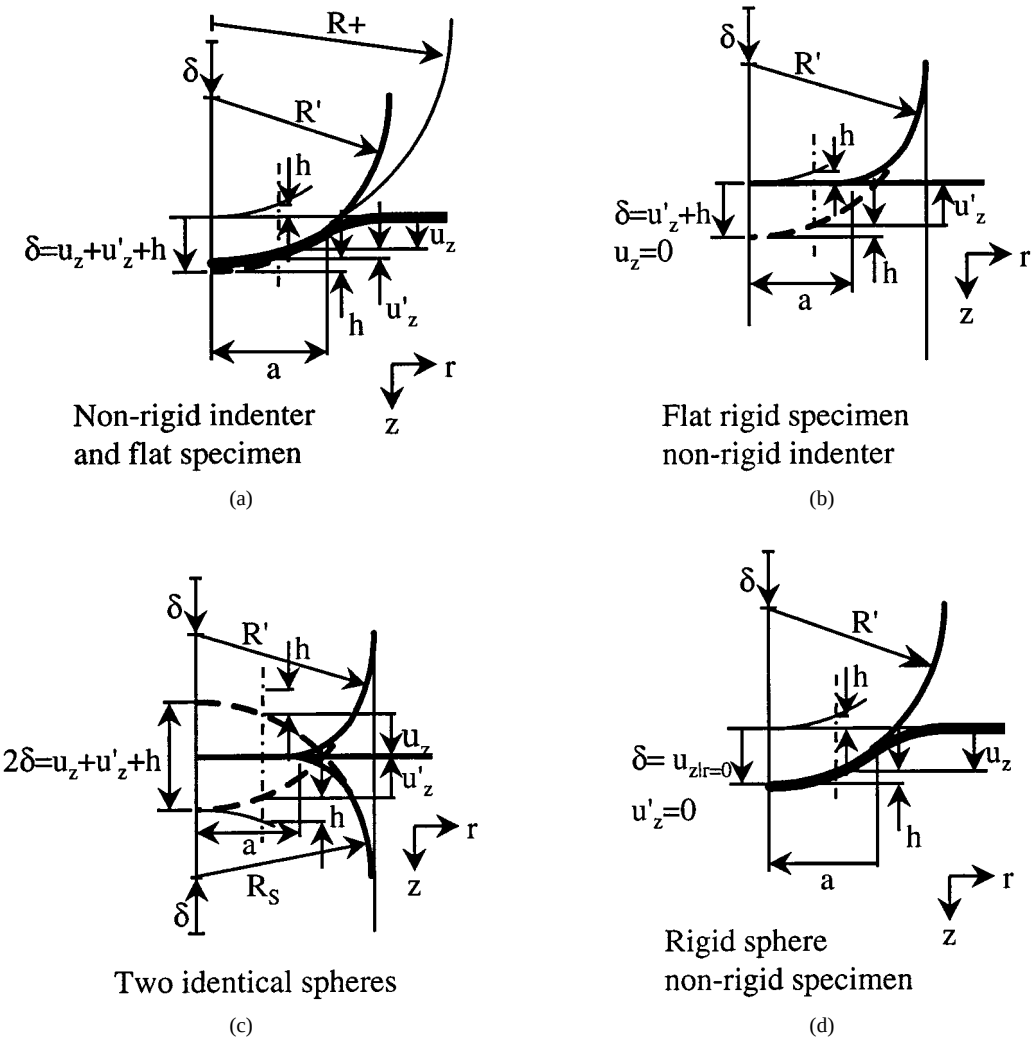

Figure 1 Schematic of contact between two elastic solids. (a) non-rigid spherical indenter and non-rigid flat specimen, (b) two identical non-rigid spheres, (c) non-rigid spherical indenter and flat rigid specimen and (d) rigid spherical indenter and flat non-rigid specimen.

the two contacting materials. For the special case of contact between a spherical indenter and a flat surface where the two materials have the same elastic properties, the radius of curvature of the contact surface is twice that of the radius of the indenter. The Hertz pressure distribution acts equally on both the surface of the specimen and the indenter, and the deflections of points on the surface of each are thus given by Equation 10. The Hertz analysis approximates the curved surface of a sphere as a flat surface since the radius of curvature is assumed to be large in comparison to the area of contact. Thus, substituting Equation 10 into Equation 9 for both u'_z and u_z and making use of Equation 7, for the general case of a non-rigid indenter and specimen, yields

$$u'_z + u_z = \left(\frac{1-\nu'}{E'} + \frac{1-\nu}{E}\right)\frac{\pi}{4a}\frac{3}{2}p_m(2a^2 - r^2) = \delta - \frac{r^2}{2R} \tag{11}$$

where R is the relative radius of curvature. With a little rearrangement, and setting $r = a$ in Equation 11, it is easy to obtain the Hertz equation, Equation 1, and to show that, at $r = 0$, the distance of mutual approach δ between two distant points within the indenter and the specimen is given by

$$\delta^3 = \left(\frac{4k}{3E}\right)^2 \frac{P^2}{R} \tag{12}$$

where k is as given in Equation 1b. Substituting Equation 1 into Equation 12, gives the distance of mutual approach, or load-point displacement, for both rigid and non-rigid indenters as

$$\delta = \frac{a^2}{R} \tag{13}$$

When the indenter is perfectly rigid, $k = 9/16(1-\nu^2)$ and the distance of mutual approach δ is equal to the penetration depth $u_{z\,|\,r=0}$ below the original specimen free surface as given by Equation 10. From Equation 10, for both rigid and non-rigid indenters, the depth of the edge of the circle of contact is exactly one half of that of the total depth of penetration beneath the surface, i.e. $u_{z\,|\,r=a} = 0.5u_{z\,|\,r=0}$.

Following Johnson [5], the quantity $E^* = 9E/16k$ may be defined such that

$$\frac{1}{E^*} = \frac{(1-\nu^2)}{E} + \frac{(1-\nu'^2)}{E'} \tag{14}$$

where Equation 12 can be written

$$\delta^3 = \left(\frac{3}{4E^*}\right)^2 \frac{P^2}{R} \tag{15}$$

The quantity E^* is the effective elastic modulus of the system and decreases as the indenter becomes less rigid. Thus, for a particular value of load P, the distance of mutual approach δ for a non-rigid indenter is greater than that for a rigid indenter due to the deformation of the indenter. For a spherical indenter, the radius of the circle of contact, a, also increases with decreasing value of E^* (or increasing value of k) as per Equation 1, and hence, for the same value of load P, the mean contact pressure is reduced. Hertz showed that, for contact between two spheres, the profile of the surface of contact was also a sphere with a radius of curvature intermediate between that of the contacting bodies and more closely resembling that body with the greatest elastic modulus. Thus, as shown in Fig. 1a, contact between a flat surface and a non-rigid indenter of radius R is equivalent to that between the flat surface and a perfectly rigid indenter of a larger radius, R^+, which may be computed using Equation 1 with k set as for a rigid indenter. If the contact is viewed in this manner, then the load-point displacement of an equivalent rigid indenter is given by Equation 10 with $r = 0$ and not Equation 15. Thus, in terms of the radius of the contact circle a and indenter load P, the equivalent rigid indenter radius is given by

$$\begin{aligned} R^+ &= \frac{3a^3 16E}{4(1-\nu^2)9P} \\ &= \frac{4Ea}{(1-\nu^2)3\pi p_m} \end{aligned} \tag{16}$$

In Equation 16, E and ν refer to materials properties of the specimen.

For the special case of the contact between two spheres of equal radii and the same elastic constants, the equivalent rigid indenter radius $R^+ \to \infty$ and the profile of the contact surface is a straight line (see Fig. 1b).

The Hertzian contact equations serve to provide information about the actual contact between elastic solids provided that deviations from the underlying assumptions previously listed are not significant. The first two assumptions concern the relative geometry of the contacting bodies, and a judgement may be made concerning the validity of these by inspection. Not so obvious is the effect of friction between the indenter and the specimen and there is considerable discussion in the literature regarding this most important issue, for example, see [6]. However, experiments [7] indicate that such interfacial friction is not significant for the case of a spherical indenter but may be significant for a cylindrical punch indenter.

2.2. Finite-element analysis

Although it is tempting to accept the predictions regarding indenter penetration depth, distance of mutual approach and radius of circle of contact given by the equations in the previous section at face value, it is nevertheless of interest to examine them either by experiment or by independent computation. In this paper, attention is given to the radius of curvature of the indented surface at a condition of full load. The objective is to test the conclusion that contact between a flat surface and a non-rigid indenter of radius R is equivalent to that between the flat surface and a perfectly rigid indenter of a larger radius R^+. Although there is no theoretical reason to doubt this result, it may not be applicable to contact involving an elastic–plastic contact. The assumption of a spherical contact surface is sometimes used as the basis for hardness theories for elastic–plastic specimen materials [8] but has not thus far been examined in detail in the literature, possibly because of the difficulty of measuring such a radius of curvature *in situ* while a load is applied to the indenter. For this reason, we have purposely not taken a direct experimental approach to the problem but address the issue via a numerical finite-element method to compute the profile of the contact surface. This numerical method of analysis had the further advantage of allowing for plastic deformation of either, or both, the specimen and the indenter in a controlled manner. Indirect verification is provided by an experimental compliance curve for a model material which exhibits clearly defined elastic and elastic–plastic contact behavior.

In the present work, the finite-element method was used to calculate the radius of circle of contact a, indentation depth u_z, distance of mutual approach δ, and effective radius R^+ for the case of a spherical indenter in contact with a flat plane specimen. Results were computed for different material characteristics corresponding to elastic and elastic–plastic contact with both relatively hard and soft indenters. Table I shows the material properties selected for analysis. The choice of material properties for the glass–ceramic material shown in Table I corresponds to those of a glass–ceramic material which, in its fired state, displays an elastic–plastic characteristic in the indentation stress field [9]. In its unfired state, the glass–ceramic has a typically brittle characteristic and the elastic modulus is comparable to that of ordinary soda–lime glass. The material properties are representative of a machinable glass–ceramic available under the trade-name "Macor" (Corning Inc.,

TABLE I Material properties for theoretical and finite-element analysis

	WC	Glass–ceramic
E (GPa)	614	64
ν	0.22	0.26
Y (MPa)	—	770

TABLE II Comparison between finite-element (FE) and theoretical results for elastic contact for WC indenter and glass-ceramic specimen with $P = 1000\,\text{N}$ and $R = 3.18\,\text{mm}$

	a (mm)	u_z (mm)	δ (mm)	R^+ (mm)
Hertz	0.3375	−0.0325	0.0358	3.518
FE	0.3359	−0.0323	0.0359	$3.516 \pm 1.0 \times 10^{-5}$
Δ (%)	−0.5	−0.8	+0.3	−0.1

TABLE III Comparison between finite-element (FE) and theoretical results for elastic contact for glass–ceramic indenter *and* specimen with $P = 1000\,\text{N}$ and $R = 3.18\,\text{mm}$

	a (mm)	u_z (mm)	δ (mm)	R^+ (mm)
Hertz	0.4441	−0.0264	0.0532	6.360
FE	0.4141	−0.0265	0.0517	$6.355 \pm 6.9 \times 10^{-6}$
Δ (%)	+0.7	+0.3	−2.8	−0.1

Corning, New York). The material properties shown in Table I for tungsten carbide (WC) correspond to those used for a rigid indenter in the experimental work to be presented in later sections.

Comparison of the various computed quantities for purely elastic contact are given in Tables II and III, where it can be seen that there is very good agreement with results of the Hertzian elastic equations in each case.

Values for R^+, the equivalent spherical indenter radius for the finite-element solutions were computed using a numerical fit to the individual node displacement results of finite-element data points. The uncertainty in this quantity is a measure of the closeness of the data to a circular arc of radius R^+. Although such a fit may be entirely appropriate for elastic contact, this is not necessarily so when plasticity is accounted for in the contact deformation, as will be seen in Section 3 below.

The profile of the specimen surface for each of the loading scenarios described above is plotted in Fig. 2. It is immediately evident that the predictions of the Hertzian analysis are indeed supported by the elastic finite-element results. The seemingly large discrepancy in the distances of mutual approach δ for the case of identical elastic properties for the indenter and specimen can be attributed to the finite-element result taking as its reference the center of the indenter, whereas the theoretical result refers to a distant point. Thus, δ for the theoretical result includes additional deflections in the "top half" of the indenter not accounted for in the finite-element model.

2.3. Experimental procedure and results

Direct measurements of the profile of the contact surface at a condition of full load are not possible due to the inaccessibility of the surface to measuring instruments. However, indirect means may be employed to validate the results of the previous section. One such means is a comparison between experimental and numerical indentation stress–strain responses. Such comparisons have been reported previously in the literature [9] for the purpose of investigating the shape of the plastic zone in

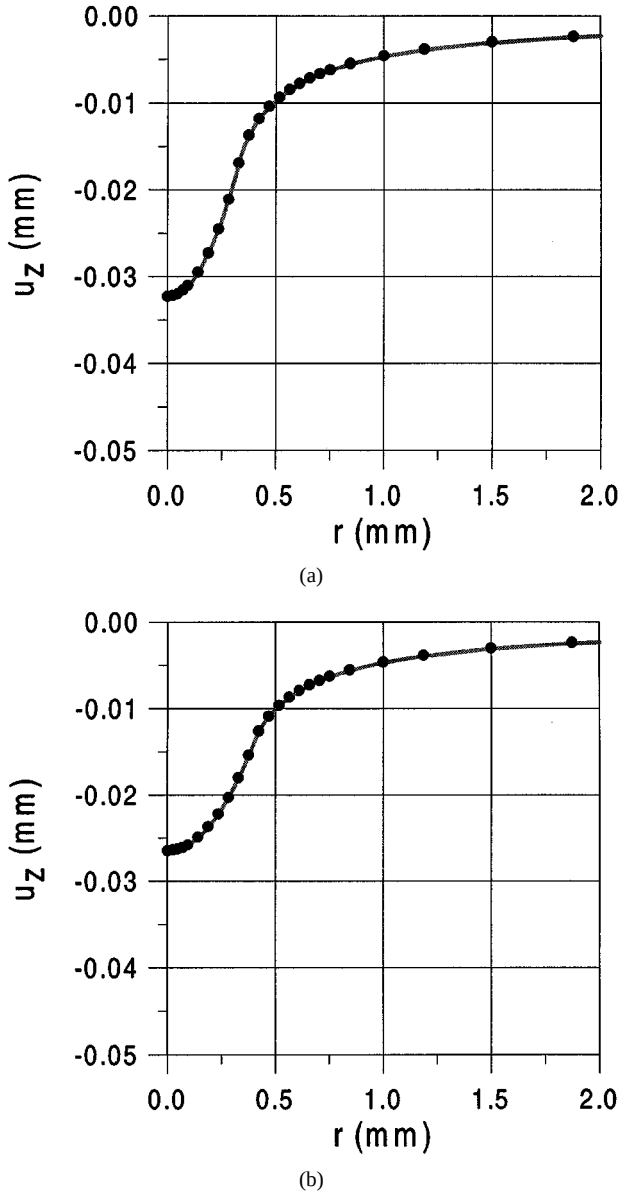

Figure 2 Displacements of the specimen surface in the vertical, or z axis, direction in the vicinity of the indenter at full load ($P = 1000\,\text{N}$, $R = 3.18\,\text{mm}$) for fully elastic material response. Solid line indicates theoretical result from Equations 10a and 10b; data points indicate finite-element results. (a) WC indenter, unfired glass–ceramic elastic specimen, and (b) unfired glass–ceramic elastic indenter and specimen.

elastic–plastic specimen materials subjected to contact loading. In the present work, we focus on a second, and perhaps more direct, method of comparison where the compliance, or depth of penetration, is measured and compared with the numerical and theoretical results.

A polished specimen of unfired glass ceramic material was mounted on the horizontal platen of a universal testing machine. The load was applied through a tungsten carbide (WC) spherical indenter of radius $R = 3.18\,\text{mm}$ by causing the crosshead of the testing machine to move downwards at a constant rate of displacement with time. A clip gauge was attached so as to measure the load-point displacement, as shown in Fig. 3. The output from the clip gauge was interfaced to a computer system which read displacement at regular time intervals during the application of load. Experimental results were compared to those computed

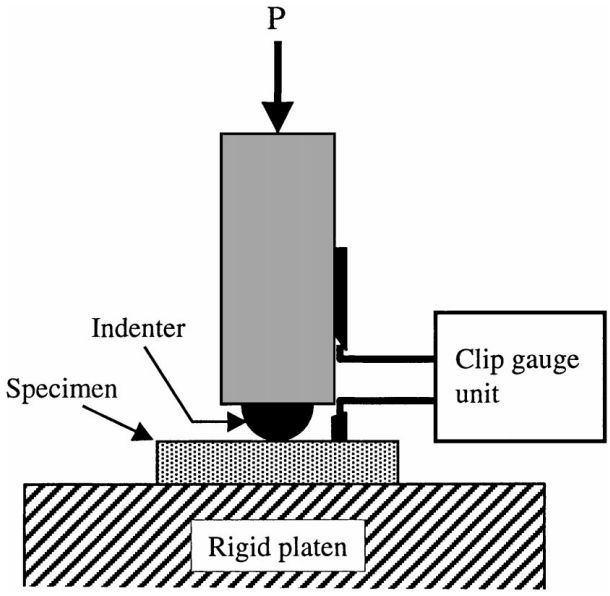

Figure 3 Schematic of experimental apparatus used for determining compliance characteristics of specimen materials. Specimen surface polished to 1 μm and placed on horizontal platen. Clip gauge is mounted between two knife edges, one touching the surface of the specimen, the other rigidly attached to the crosshead post. Load P applied to the indenter via crosshead on universal testing machine.

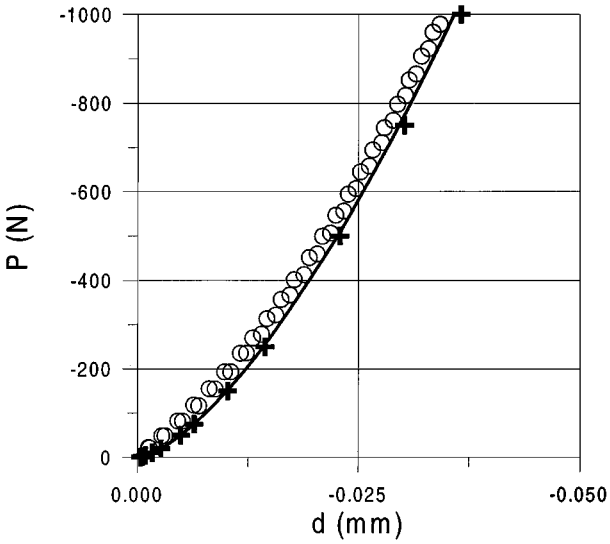

Figure 4 Compliance curves for elastic response showing (solid line) Hertz elastic response, (+) finite element and (O) experimental results for WC elastic indenter and unfired glass–ceramic elastic specimen.

using Equation 12 and those obtained using the finite-element method described in Section 2.2. Fig. 4 shows that there is good agreement between the load versus displacement characteristics obtained by each of the three methods.

3. Contact between elastic–plastic solids

3.1. Analysis

In the preceding sections, the Hertzian elastic contact equations were reviewed and verified using finite-element analysis. However, despite there being considerable discussion in the literature, there appears to be little agreement between the essential features concerning the nature of elastic–plastic contact. The characteristics of elastic–plastic contact appears to be almost certainly dependent upon the ratio of the yield stress to the elastic modulus of the specimen material. This dependence was studied in an earlier publication [9] where it was found that for materials with a high value of E/Y, such as a ductile metal, the shape of the plastic zone appeared to be hemispherical and in agreement with the so-called "expanding cavity model" of Johnson [5]. For a material with a low value of E/Y, such as the glass–ceramic considered here, the shape of the plastic zone was fully contained within the contact radius at the specimen surface and appeared to be similar to that reported by the elastic–constraint model of Shaw and De Salvo [10]. A consistent theoretical model for indentation contact which embraces the range of material properties usually encountered in engineering materials has yet to be formulated. Such a theoretical treatment may rely on there being an accurate knowledge of the indentation profile in the fully loaded condition, hence the motivation for the present work.

3.2. Finite-element analysis

Theoretical analysis of an elastic–plastic indentation with a spherical indenter is difficult because of the uncertainty regarding the shape of the evolving plastic zone. However, the problem is suitable for analysis using the finite-element method where no assumption about the shape of the zone need be made beforehand. In the present work, plastic or non-linear specimen behavior was included by specifying an elastic–perfectly–plastic uniaxial stress–strain relationship as part of the property set for the elements representing the specimen. It is assumed that such a relationship is representative of that of the actual specimen material. A special feature of the present analysis is that, by the use of special gap elements, the expanding area of contact is accommodated automatically and no knowledge of the radius of the contact circle is required *a priori*. Elastic–plastic behavior is modeled here by treating the specimen material as a non-linear elastic solid. Hence, only the application of load may be considered, but since the radius of curvature of the indented surface at full load is of primary concern, it is not necessary to consider the unloading portion of the contact event.

The finite-element analysis presented here initially assumes a perfectly elastic, relatively hard, spherical indenter in frictionless contact with the flat surface of an elastic–plastic specimen. Full details of the finite-element procedure are to be reported elsewhere [11] and need not be repeated here. Elastic–plastic behavior was accommodated by an iterative procedure involving a secant method of adjustment to the local stiffness of plate elements in which plasticity, according to the Tresca criterion, was satisfied within a specified tolerance level. In the secant method, the elastic modulus is given by the slope of a straight line drawn between the origin and the point on the stress–strain curve rather than the local slope of the stress–strain curve at that point.

As well as the more usual analysis involving a hard, spherical indenter and an elastic–plastic specimen, we

TABLE IV Comparison between finite-element (FE) results for a WC indenter and an elastic–plastic glass–ceramic specimen and theoretical results for purely elastic contact with $P = 1000$ N and $R = 3.18$ mm

	a (mm)	u_z (mm)	δ (mm)	R^+ (mm)
Hertz	0.3375	−0.0325	0.0358	3.518
Elastic–plastic	0.4766	−0.0464	0.0485	3.257
FE result				$\pm 2.2 \times 10^{-5}$
Δ (%)	+29.2	+50.6	+26.1	−8.0

TABLE V Comparison between finite-element (FE) results for glass–ceramic elastic–plastic indenter *and* specimen and theoretical results for purely elastic contact with $P = 1000$ N and $R = 3.18$ mm

	a (mm)	u_z (mm)	δ (mm)	R^+ (mm)
Hertz	0.4111	−0.0264	0.0532	6.360
Elastic–plastic	0.4922	−0.0311	0.0599	6.142
FE result				$\pm 7.6 \times 10^{-5}$
Δ (%)	+16.5	+28.6	+11.2	−3.6

also consider the case of an indenter having the same elastic–plastic properties of the indenter. In both cases, there is no *a priori* reason to expect that the profile of the contact surface has a constant value of radius of curvature when plastic deformation occurs within the specimen, the indenter, or both. Calculations were performed with elastic constants as specified in Table I (and as also used in the elastic computations of Section 2.2.) with the additional inclusion of a yield stress for the indenter and specimen material. The yield stress, Y, was estimated from a consideration of the Vickers hardness value and the deviation from linearity in an indentation stress–strain response as previously reported [9]. A comparison between various calculated quantities are given in Tables IV and V, and the difference between the profiles of the elastic and elastic–plastic deformations are shown in Fig. 5.

Again, values for R^+ for the finite-element result were computed using a numerical fitting procedure to the individual node displacements of the finite-element results. Although in the case of elastic–plastic contact there is no reason to assume that the indentation profile is of a constant radius of curvature, we compute this quantity, together with the uncertainty, for comparison purposes with the fully elastic case.

3.3. Experimental procedure and results

Compliance characteristic curves were obtained using the apparatus described in Section 2.3. Fig. 6 shows experimental and finite element results. Also shown in Fig. 6 is the Hertzian elastic response for comparison purposes. Deviation from the Hertzian elastic conditions is indicative of a plastic event within the specimen material.

4. Discussion

For the elastic contact, it is of course not surprising that the penetration depth and radius of circle of contact in Tables II and III for the WC indenter are greater than

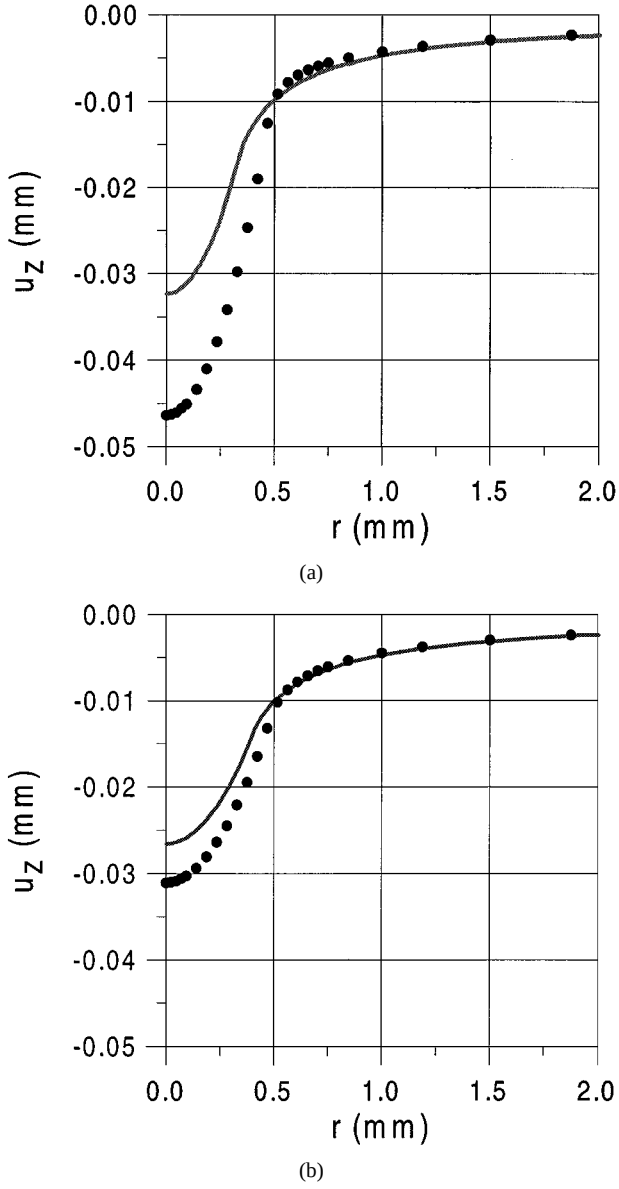

Figure 5 Displacements of the specimen surface in the vertical, or z axis, direction in the vicinity of the indenter at full load ($P = 1000$ N, $R = 3.18$ mm) for elastic–plastic response. Solid line indicates theoretical result from Equations 10a and 10b, data points indicate finite-element results. (a) WC elastic indenter, glass–ceramic elastic-plastic specimen, and (b) glass–ceramic, elastic–plastic indenter and specimen.

those computed for the case of a glass–ceramic indenter, since the elastic modulus of the former is considerably larger than that of the latter. Of particular interest is the radius of curvature of the deformed surface R^+. In the case of the WC indenter, R^+ is closer in magnitude to the undeformed indenter radius $R = 3.18$ mm compared to the case of the glass–ceramic indenter since the elastic stiffness of the glass-ceramic is very much less than that of WC. This is consistent with the original analysis of Hertz [1, 2]. Tables II and III show that there is close agreement between the results of the finite-element analysis and the theoretical equations. The compliance curves in Fig. 3 demonstrates a good agreement between the finite-element results, theory and experiment.

Of further interest is the profile of the deformed surfaces when plastic deformation occurs in the specimen material. There is, not surprisingly, a considerable

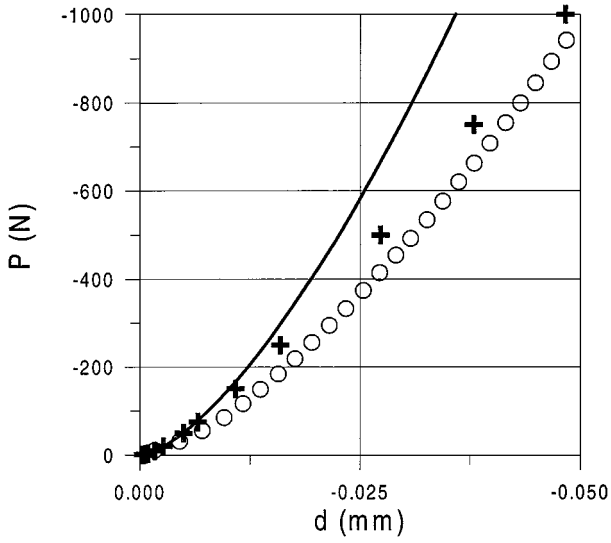

Figure 6 Compliance curves showing (solid line) Hertz elastic response, (+) finite element and (O) experimental results for a WC elastic indenter and glass–ceramic elastic–plastic specimen.

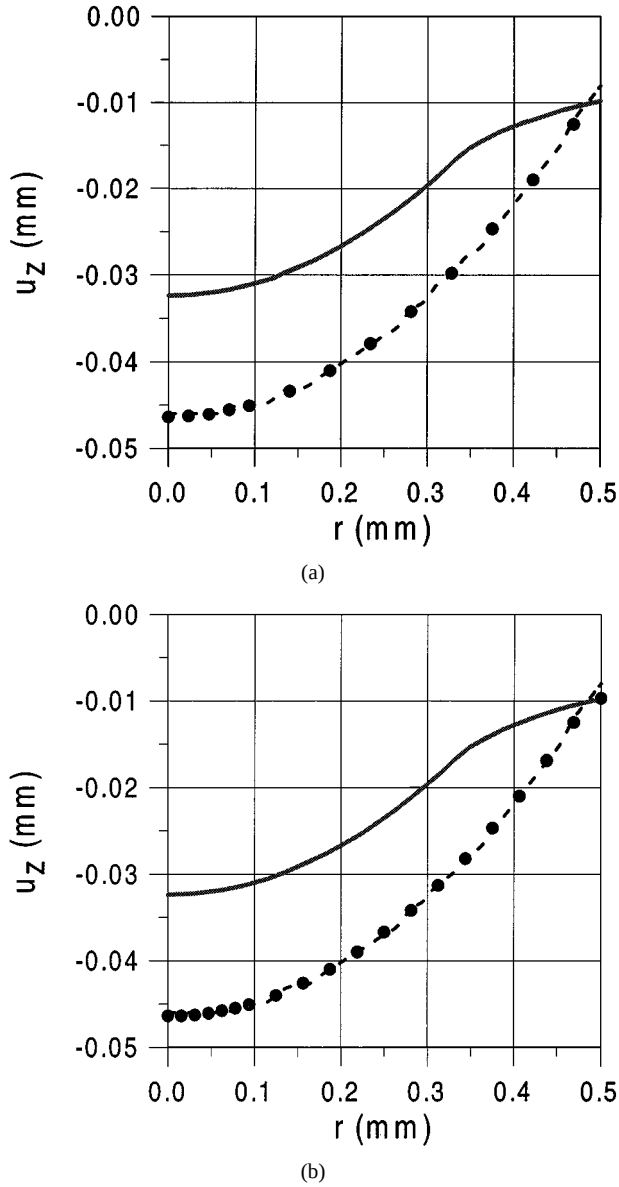

Figure 7 Displacements of the specimen surface in the vertical, or z axis, direction in the vicinity of the contact surface at full load ($P = 1000$ N, $R = 3.18$ mm) for elastic–plastic response. Solid line indicates theoretical result from Equations 10a and 10b, data points indicate finite-element results as per Fig. 5 and dashed line is the spherical contact surface computed using values of R^+ fitted to finite-element results. (a) WC elastic indenter and glass–ceramic, elastic–plastic specimen, and (b) glass–ceramic, elastic–plastic indenter and specimen.

increase in the penetration depth since, due to plastic deformation, the same indenter load has now to be supported by strains elsewhere in the specimen material rather than immediately beneath the indenter. The finite-element results suggest that the indentation surface does have a spherical profile, as indicated by the very low uncertainty in the fitted value of the effective radius R^+. Table IV shows that although there is a considerable discrepancy between the effective radius R^+ as calculated using Equation 16, as would be expected since Equation 16 assumes no plastic deformation, the results show that the profile of the surface beneath the indenter is indeed spherical, but with a smaller radius of curvature than that predicted by Equation 16. Although we might expect an axis-symmetric profile, e.g. elliptical, there is no *a priori* reason to expect a spherical profile. In the absence of any supporting theoretical treatment, the compliance curves shown in Fig. 6 show that the finite-element results are supported, indirectly, by experimental evidence. The differences between the finite-element and the experimental results, estimated at about 5%, in Fig. 6 probably arise due to the adoption of the Tresca criterion for plasticity, an elastic–perfectly–plastic stress–strain characteristic and the error associated with the yield stress of the experimental material in the finite-element analysis.

When plasticity occurs in both specimen and indenter, the shape of the deformed surface cannot be assumed *a priori* to be spherical, but the results, as indicated by the uncertainty in R^+ in Table V, suggest that it is so. Again, there is a large discrepancy with R^+ as calculated by Equation 16, but this is not surprising considering that Equation 16 applies to purely elastic contact. These conclusions are further illustrated in Fig. 7, where the profile for the indentation surface beneath the indenter, at full load, for elastic contact, elastic–plastic specimen and elastic-plastic specimen and indenter are presented together with a profile generated using the finite-element estimations of R^+.

It will be recalled that the Hertz analysis shows that indentation with an indenter of radius R of a given elastic modulus is equivalent to indentation with a perfectly rigid indenter of larger radius R^+. In the present work, the validity of this result has been verified by independent computation. It has also been shown that indentations involving elastic–plastic deformations are equivalent to indentations with a perfectly rigid indenter of radius R^+ whose value is somewhat smaller than that calculated using the Hertz equations for elastic contact. Thus, indentation theories which rely on the indented surface being spherical are vindicated in this regard.

Acknowledgements

The author wishes to acknowledge M. V. Swain and R. W. Cheary for advice and useful discussions regarding this work.

References

1. H. HERTZ, *J. Reine Angew. Math.* **92** (1881) 156; Translated and reprinted in English in "Hertz's Miscellaneous Papers" (Macmillan & Co, London, 1896) Ch. 5.
2. H. HERTZ, *Verhandlungen des Vereins zur Beförderung des Gewerbe Fleisses* **61** (1882) 410; Translated and reprinted in English in "Hertz's Miscellaneous Papers" (Macmillan & Co, London, 1896) Ch. 6.
3. F. GUIBERTEAU, N. P. PADTURE, H. CAI and B. R. LAWN, *Philos. Mag. A* **68** (1993) 1003.
4. M. BARQUINS and D. MAUGIS, *J. Mec. Theor. Appl.* **1** (1982) 331.
5. K. L. JOHNSON, in "Contact Mechanics" (Cambridge University Press, 1985).
6. D. A. SPENCE, *J. Elast.* **5** (1975) 297.
7. A. C. FISCHER-CRIPPS and R. E. COLLINS, *J. Mater. Sci.* **29** (1994) 2216.
8. J. S. FIELD and M. V. SWAIN, *J. Mater. Res.* **8** (1993) 297.
9. A. C. FISCHER-CRIPPS, *J. Mater. Sci.* **32** (1996) 727.
10. M. C. SHAW and D. J. DESALVO, *Trans. ASME, J. Eng. Ind.* **92** (1970) 469.
11. G. CARÈ and A. C. FISCHER-CRIPPS, *J. Mater. Sci.* **32** (1997) 5653–5659.

Received 20 October 1997
and accepted 19 August 1998